Dalton Transactions

Accepted Manuscript

ROYAL SOCIETY OF CHEMISTRY

www.rsc.org/dalton

Journal Name

RSCPublishing

ARTICLE

Facile Fabrication and Enhanced Photosensitized Degradation Performance of g-C_3N_4-$Bi_2O_2CO_3$ Composite

Cite this: DOI: 10.1039/xoxxoooooox

Received ooth January 2012,
Accepted ooth January 2012

DOI: 10.1039/xoxxoooooox

www.rsc.org/

Miao Xiong,[a,c] Lang Chen,[a,c] Qing Yuan,[a] Jie He,[a] Sheng-Lian Luo,[a] Chak-Tong Au[a,b] and Shuang-Feng Yin[a,*]

Flower-like $Bi_2O_2CO_3$ and g-C_3N_4-$Bi_2O_2CO_3$ microspheres with high adsorption ability were synthesized using a facile method, and their dye-induced photosensitized degradation activity under visible light irradiation was evaluated. The as-synthesized samples were characterized by XRD, FT-IR, FESEM, TEM (HRTEM), UV-vis DRS and nitrogen adsorption-desorption techniques. It was found that the activity of $Bi_2O_2CO_3$ was significantly enhanced due to the generation of g-C_3N_4-$Bi_2O_2CO_3$ heterostructures. The dye-sensitization and presence of g-C_3N_4 are beneficial for the visible-light excited process. The enhancement of photocatalytic performance is ascribed to a proper matching of the energy levels of dye, $Bi_2O_2CO_3$ and g-C_3N_4 that facilitates the separation and transfer of photogenerated electrons and holes at the heterojunctions. The results of the present study give insights that are beneficial for the design of heterostructured materials.

Introduction

To treat wastewater contaminated with organic chemicals by photocatalytic degradation is promising for environmental remediation.[1] The success of the technology depends on the development of semiconductors that are high in visible-light-driven performance. Among them, the hetero-nanostructured catalysts are attractive because they broaden the range of visible-light absorption, and are efficient in terms of the separation and transfer of photogenerated electrons and holes.[2-4] Recently, we synthesized Ag/$BiVO_4$,[5] $Bi_2O_2CO_3$/BiOI,[6] and Bi_2O_3/$BiVO_4$[7] composites. When used as photocatalysts under the irradiation of visible light, they exhibit activities higher than those of their components due to the presence of heterojunctions. Meanwhile, it has been reported that dye sensitization is a way for the photodegradation and mineralization of dyes.[8,9] With the dye molecules attached on the surface of the semiconductor, they are excited under the irradiation of visible light, and there is the transfer of photogenerated electrons from the excited dye molecules to the conduction band of the semiconductor. It is envisioned that it is possible to improve the separation of the charge carriers and to enhance visible light absorption by designing a hybrid photocatalyst that combines the merits of hetero-structure and dye sensitization.

$Bi_2O_2CO_3$ (BOC) exhibits strong absorption in the ultraviolet region and is superior to P25 in photocatalytic performance.[10] Its practical application, however, is severely constrained because BOC is poor in absorption of visible light. It was reported that by coupling BOC with a semiconductor of narrow band gap, one can synthesize nanocomposites having heterostructures capable of harvesting visible light as well as showing effective separation of photogenerated charge carriers.[6,11] In our previous work, it was found that Rh-B can be degraded under visible light irradiation over BOC of wide band gap (3.4 eV), and the process could be a dye-sensitized one.[6] Graphitic carbon nitride (g-C_3N_4) is a low-cost substance that shows high thermal and chemical stability as well as amenability towards chemical modification.[12] Due to its narrow band gap (~ 2.7 eV), it is suitable for visible-light photocatalysis. It is widely used as sensitizer to realize the visible-light response of semiconductors with wide band gap through the formation of heterostructures, for instance, g-C_3N_4-ZnO,[13] g-C_3N_4-$BiPO_4$,[14] g-C_3N_4-BiOBr[15] and g-C_3N_4-Bi_2WO_6[16]. After considering the energy levels of g-C_3N_4 and BOC, we envisaged that the coupling of the two would end up with a double-sensitizer system, ideal for achieving high visible-light-driven photocatalytic performance.

In this work, flower-like $Bi_2O_2CO_3$ and g-C_3N_4-$Bi_2O_2CO_3$ microspheres with high adsorption ability were synthesized, and characterized by XRD, FT-IR, FESEM, TEM (HRTEM), UV-vis DRS and nitrogen adsorption–desorption techniques. In addition, the photocatalytic mechanism over g-C_3N_4-$Bi_2O_2CO_3$ was investigated. As expected, visible-light-driven activity was enhanced by introducing a proper amount of g-C_3N_4 into BOC due to the formation of g-C_3N_4-$Bi_2O_2CO_3$ heterostructures. By varying the reaction conditions, we found that the photocatalytic degradation of dyes over g-C_3N_4-$Bi_2O_2CO_3$ under visible light is a dye-sensitized process.

Experimental section

Preparation:

All reagents were of analytical grade and were used without further purification. We synthesized g-C_3N_4 through direct heating of melamine.[17] Typically, 5 g melamine powder was put into an alumina crucible and heated to 500 ^oC (heating rate = 2 ^oC min^{-1}) for a 2-h stay at this temperature, then heated to 530 ^oC for another 2-h period. After cooling to room temperature, g-C_3N_4 was obtained in powder form.

The typical preparation of g-C_3N_4-$Bi_2O_2CO_3$ photocatalysts was as follows: 0.5 g CTAB (Hexadecyl trimethyl ammonium Bromide) and 2.997 g Na_2CO_3 were added to 90 mL distilled water, followed by the addition of an appropriate amount of g-C_3N_4. The mixture was subject to 40-min ultrasonic treatment for complete dispersion of g-C_3N_4. Then a solution of 1.712 g $Bi(NO_3)_3$•$5H_2O$ dissolved in 10 mL HNO_3 (1 $molL^{-1}$) was added dropwise under vigorous stirring. After being stirred for 2 h, the product was harvested by filtration, washed several times with distilled water and ethanol, and finally dried at 60 ^oC overnight. The as-synthesized g-C_3N_4-$Bi_2O_2CO_3$ composites with g-C_3N_4 percentage of 5 wt.%, 10 wt.% and 15 wt.% are denoted hereinafter as 5% CN-BOC, 10% CN-BOC and 15% CN-BOC, respectively. BOC was synthesized according to the above procedures but without the addition of g-C_3N_4.

Characterization:

Powder X-ray diffraction (XRD) data of the as-prepared samples were recorded on a Bruker Automatic Diffractometer (Cu-Kα radiation, λ=0.154056 nm) using a step scan mode in the 2θ=10-80^o range. Fourier transform spectrophotometry (FT-IR, VERTEX 70, Bruker) using KBr as reference was performed for FT-IR measurement. The micro- and nano-structure as well as the morphology of the as-prepared samples were examined using a field emission scanning electron microscope (FE-SEM) (Hitachi S-4800). Transmission electron microscopy (TEM) and high-resolution transmission electron microscopy (HRTEM) images were taken over a JEOL 3010 transmission electron microscope at 200 kV. The BET surface area was measured using a Quantachrome Nova Win instrument. The UV-vis diffuse reflectance spectra were recorded at room temperature on a Cary-100 spectrophotometer, using $BaSO_4$ as reference.

Photocatalytic tests:

The photocatalytic activities of the as-prepared samples were evaluated in a glass reactor. Several kinds of dyes, rhodamine-B (Rh-B, 2×10^{-5} $molL^{-1}$), methylene blue (MB, 2×10^{-5} $molL^{-1}$), crystal violet (CV, 2×10^{-5} $molL^{-1}$) or methylene orange (MO, 2×10^{-5} $molL^{-1}$) was used to evaluate the activity of the as-prepared samples. In each experiment, 0.05 g of the sample was dispersed in 100 mL aqueous solution containing the dye. A 300 W Xe lamp equipped with a cutoff filter was used as the light source to provide visible light irradiation (λ ≥ 400 nm). Prior to irradiation, the reaction solutions were magnetically stirred in the dark for 30 min to obtain the saturated adsorption of dye onto the catalysts. At certain time intervals, 4 mL aliquots were sampled and centrifuged to remove the catalyst. The concentration of the dye was analyzed by recording the absorbance at the characteristic band using a Cary-100 UV−vis spectrophotometer.

Results and discussion

Physicochemical properties:

From the XRD patterns (Figure 1), one can see narrow and sharp peaks characteristic of tetragonal BOC (JCPDS 41-1488). The two distinct peaks at 2θ = 13.08° and 27.41° can be indexed as the (100) and (002) diffractions of g-C_3N_4 (Figure 1f).[18,19] The XRD patterns of 5% CN-BOC, 10% CN-BOC and 15% CN-BOC samples are rather similar to that of BOC, and there is no detection of the characteristic peaks of g-C_3N_4, indicating high dispersion of g-C_3N_4.

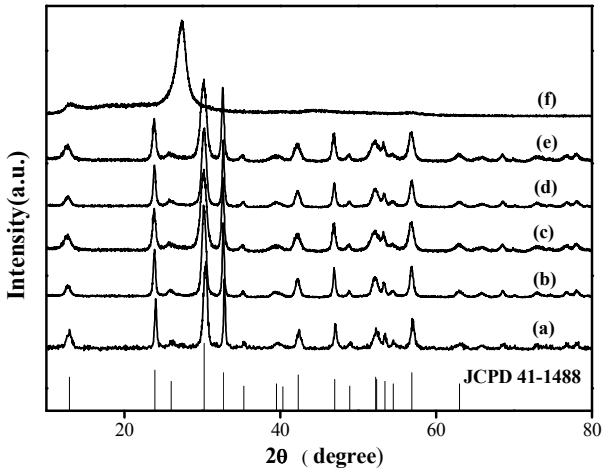

Figure 1. XRD patterns of (a) BOC, (b) 5% CN-BOC, (c) 10% CN-BOC, (d) 15% CN-BOC and (e) 10% CN-BOC after five recycle runs; (f) g-C_3N_4 photocatalysts

Figure 2 displays the FT-IR spectra of g-C_3N_4, BOC, and 10% CN-BOC. The intense bands in the 1200-1650 cm^{-1} region are typical stretching modes of C-N heterocycles.[20,21] The peak at 1637 cm^{-1} is attributable to C-N stretching vibration mode, while those at 1246, 1322, 1411 and 1560 cm^{-1} are associated with aromatic C-N stretching.[22] The band near 808 cm^{-1} is attributed to out-of-plane bending modes of heterocyclic C-N.[23] For BOC, the two intense peaks at 1391 and 1468 cm^{-1} are assigned to the anti-symmetric vibration ν3 mode of CO_3^{2-}, while the peaks at 1068 and 846 cm^{-1} are ascribed to the symmetric stretching ν1 and the out-of-plane bending ν2 modes of CO_3^{2-}, respectively.[24] In addition, the broad band at 3442 cm^{-1} is due to physically adsorbed H_2O.[25] The 10% CN-BOC sample shows the characteristic absorption bands of g-C_3N_4 and BOC, confirming the co-presence of g-C_3N_4 and BOC. The results evidence the successful introduction of g-C_3N_4 into BOC.

Figure 3 shows the SEM images of BOC and 10% CN-BOC. One can see that BOC has flower-like morphology with diameter around 1.5 micrometers. The loosely packed BOC microspheres are assembled from uniformly distributed nanoplates that are about several nanometers in thickness. Although there is no change on the morphology and size of the microspheres after the introduction of g-C_3N_4 into BOC, the nanoplates assembled into the 10% CN-BOC sample are not uniform, and there is the stacking of irregular nanoplates on the surface of the flower-like microspheres.

The TEM image (Figure 4a) of 10% CN-BOC shows a flower-like morphology, consistent with the SEM results. The HRTEM image of 10% CN-BOC reveals a lattice spacing of 0.327 nm that can be ascribed to the (002) plane of hexagonal g-C_3N_4 (JCPDS 87-1526). The lattice fringes have a spacing of 0.297 nm, corresponding to the (110) plane of tetragonal BOC (JCPDS 41-1488). According to the SEM and TEM images, it can be inferred that there is the aggregation and embedment of

g-C_3N_4 on the surface of BOC during the formation of the flower-like structures. The close interaction between g-C_3N_4 and BOC enables fast transfer of electrons during photo excitation processes.

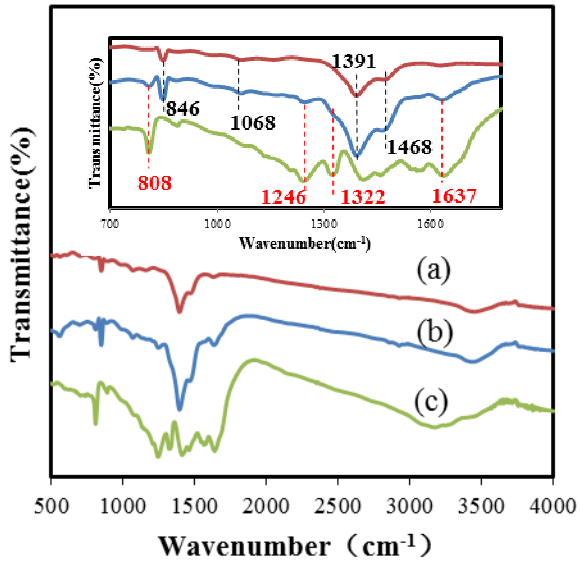

Figure 2. FT-IR spectrum of (a) BOC, (b) 10% CN-BOC and (c) g-C_3N_4

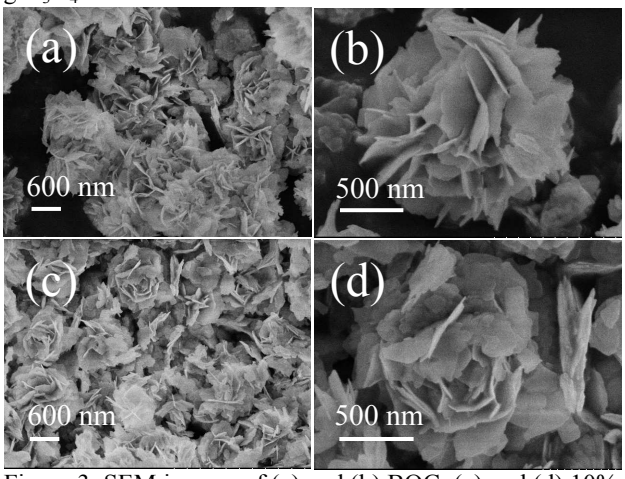

Figure 3. SEM images of (a) and (b) BOC; (c) and (d) 10% CN-BOC samples

Depicted in Figure 5 are the UV-visible diffuse reflectance spectra of the as-prepared samples. BOC and g-C_3N_4 show absorption edges at 380 and 470 nm, respectively, indicating that BOC cannot be excited by light with $\lambda \geq 400$ nm. With increasing of g-C_3N_4 mass ratios, there is red shift of UV-vis absorption edge. In general, the optical absorption performance of a semiconductor is evaluated based on band gap energy (E_g).[26,27] For a crystalline semiconductor, the optical absorption near band edge follows the formula $(\alpha h\nu)^n = A(h\nu - E_g)$ where α, h, ν, E_g, and A are the absorption coefficient, Plank constant, light frequency, band gap, and a constant, respectively. Among them, n is 2 for direct inter-band transition and 1/2 for indirect inter-band transition. For BOC, the value of n is 2 for direct inter-band transition.[26,27] The E_g value can be estimated by extrapolating the straight portion of "$(\alpha h\nu)^2 - h\nu$" plot to the $\alpha = 0$ point. The band gap of BOC is 3.21 eV, quite consistent with the reported values.[27] As for g-C_3N_4, the band gap is estimated to be 2.7 eV, showing an intrinsic semiconductor-like absorption in the blue region of the visible spectrum.[28]

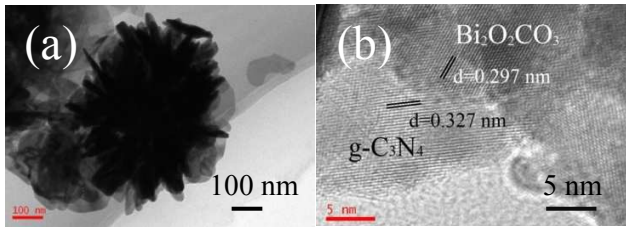

Figure 4. (a) TEM image and (b) HRTEM image of the 10% CN-BOC composite

Photocatalytic property:

The photocatalytic activity of the as-prepared samples was studied for the degradation of Rh-B under visible light ($\lambda \geq 400$ nm) irradiation. The UV-vis absorption spectra show that the characteristic band of Rh-B (centered at 553 nm) declines rapidly and disappears upon visible light irradiation over BOC and 10% CN-BOC (Figures S1 and S2, respectively; see electronic supplementary information, ESI). As shown in Figure 6, it is clear that all the CN-BOC composites show higher activities than g-C_3N_4 or $Bi_2O_2CO_3$. The photocatalytic degradation of organic pollutants generally follows kinetics of pesudo-first order,[9] and the degradation rate is evaluated by the reaction constant k, whereas the constant k can be determined by plotting $\ln(C/C_0)$ against irradiation time. Upon increase of g-C_3N_4 amount from 5 to 10 wt.%, there is enhancement of photocatalytic activity. Among them, 10% CN-BOC shows the highest activity (k=0.0512 min^{-1}), which is about 2 times that of BOC (k=0.0318 min^{-1}) and 4 times that of g-C_3N_4 (k=0.0126 min^{-1}). It was found that there is 32%, 37%, 45% and 33% Rh-B adsorption on BOC, 5% CN-BOC, 10% CN-BOC, and 15% CN-BOC, respectively, revealing the close relationship between Rh-B adsorption ability and photocatalytic performance of the as-prepared catalysts: the higher amount of Rh-B adsorption, the higher is the degradation rate. It is reckoned that nanomaterials of large specific surface area are high in adsorption ability.[29] The specific surface areas of BOC, 5% CN-BOC, 10% CN-BOC, and 15% CN-BOC are 25.6, 29.3, 37.2, and 26.3 m^2g^{-1}, respectively, showing a trend matching the results of Rh-B adsorption. Despite strong in visible light absorption, g-C_3N_4 by itself is relatively low in photocatalytic activity, only 40% of the original Rh-B is removed within 30 min of irradiation. Unlike g-C_3N_4, BOC with wide band gap (3.21 eV) shows much higher activity under visible light irradiation.

To find out whether it is Rh-B, BOC or CN-BOC that is excited in the degradation process, the process was conducted under irradiation of monochromatic visible light. The incident light was kept at $\lambda = 550 \pm 15$ nm, at which only Rh-B molecules are excited, while both g-C_3N_4 and BOC have no response at this region. As shown in Figure 7, the photolysis of Rh-B without a photocatalyst under the monochromatic light is negligible. Furthermore, it takes 120 and 100 min for complete removal of Rh-B over BOC and 10% CN-BOC, respectively, longer than that under the irradiation source of $\lambda \geq 400$ nm. This could be due to the difference in irradiation intensity. Nonetheless, it is worth pointing out that 80% of Rh-B can be removed over BOC in 100 min under monochromatic light irradiation. These results indicate that dye sensitization plays a major role in the photo-degradation process. Moreover, the photo-degradation of Rh-B over 10% CN-BOC is faster than that over BOC under the irradiation of monochromatic visible

light (λ = 550±15 nm), and the phenomenon is attributable to the enhanced adsorption of Rh-B on 10% CN-BOC. It is hence deduced that the degradation of Rh-B over BOC is a dye-sensitization process, and can be enhanced by loading a proper amount of g-C_3N_4 on BOC.

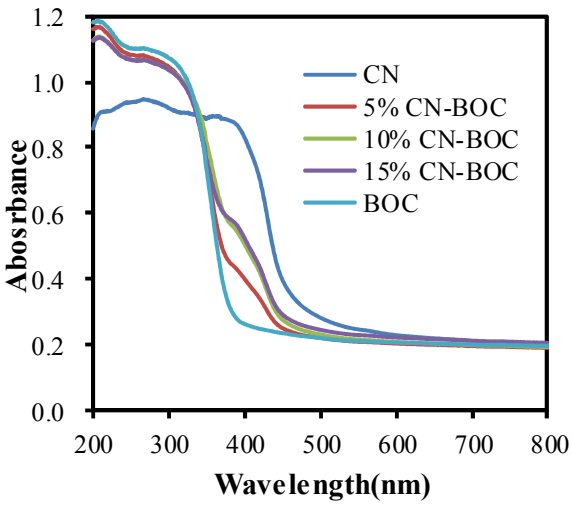

Figure 5. UV-vis diffuse reflection spectra of g-C_3N_4 as well as BOC and CN-BOC composites

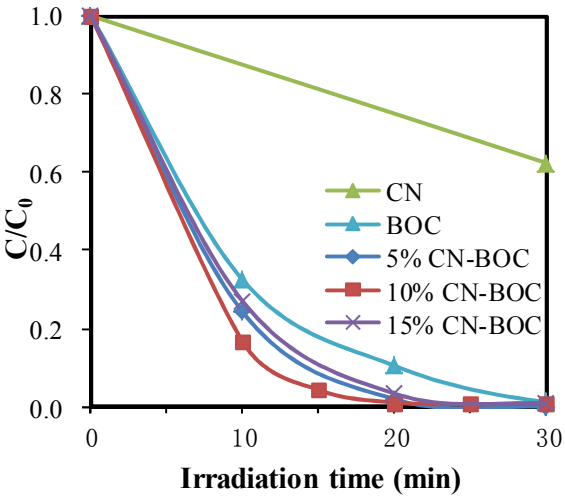

Figure 6. Degradation rates of Rh-B under visible light irradiation in the presence of g-C_3N_4, BOC and CN-BOC

In addition, 10% CN-BOC was examined for degradation of other cationic dyes (MB and CV) (Figures S3-S4, ESI). One can see that the characteristic absorption peaks intensity of the cationic dyes decreases gradually and disappears finally, indicating that the catalyst exhibits wide applications for the degradation of cationic dyes. It was reported that dye-sensitization photocatalysts could be limited to the degradation of anionic dyes.[8,9] In our case, 10% CN-BOC can be applied for the photo-degradation of anionic dyes (MO) under the irradiation of visible light (Figure S5, ESI). It hence has advantage over the photosensitized catalysts that can only be applied for the degradation of cationic dyes. It is considered that the 10% CN-BOC photocatalyst is versatile for the treatment of waste water.

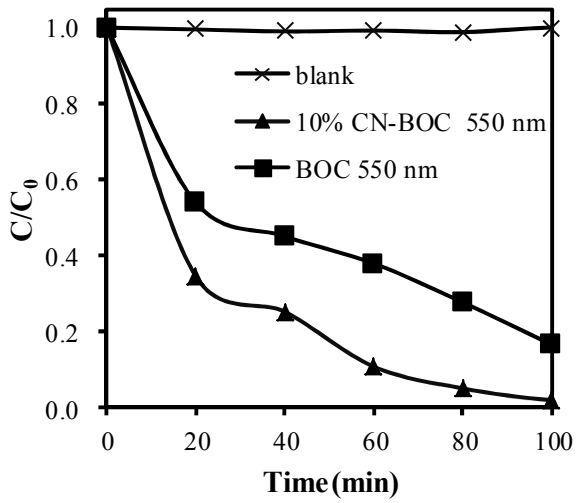

Figure 7. Photocatalytic degradation of Rh-B aqueous solution in the presence of BOC and 10% CN-BOC photocatalyst under monochromatic visible light irradiation (λ = 550±15 nm)

Photocatalytic mechanism

Depending on the reaction mechanism, a photocatalytic process involves active species that can be different from those of the others. To understand the reaction mechanism, it is important to identify the active species that participate in the photocatalytic processes. By means of trapping experiments, species such as holes, hydroxyl radicals (•OH) and superoxide radicals ($•O_2^-$) can be identified using triethanolamine (TEOA),[18] tertbutyl alcohol (TBA) [30] and benzoquinone (BQ) [31] as scavenger, respectively. As shown in Figure 8, after adding TBA, there is no significant change in terms of the degradation of Rh-B, suggesting that •OH is not the main kind of active species. When TEOA is used as holes scavenger, the photocatalytic reaction over 10% CN-BOC is significantly quenched. It is worth pointing out that with the addition of TEOA, there is sharp decrease in the extent of Rh-B adsorption (from 45% to 7%), meaning that the dye-sensitization process is negligible, while g-C_3N_4 in the composite which can be excited under visible light plays a main role in Rh-B photo-degradation. Therefore, the result confirms that holes originated from g-C_3N_4 excitation are the main active species. In addition, once BQ is added to the reaction system, the degradation efficiency of Rh-B is lowered significantly despite there is a rise in Rh-B adsorption. The result demonstrates that $•O_2^-$ entities are also active species. It is well known that $•O_2^-$ is formed in photocatalytic processes when an oxygen molecule adsorbed on the surface of catalyst takes up a photogenerated electron.[1,8] In other words, photogenerated electrons also play an important role in dye degradation over 10% CN-BOC.

Based on the above results, it is deduced that in the g-C_3N_4-$Bi_2O_2CO_3$ photocatalytic system the degradation of dye is a photosensitized process, and both holes and $•O_2^-$ (not •OH) are active species. A schema for electron-hole separation and transportation at the g-C_3N_4/$Bi_2O_2CO_3$ interfaces is proposed (Scheme 1). The valence band (VB) and conduction band (CB) of BOC estimated according to the Mulliken electronegativity theory[32] are located at 3.44 and 0.23 eV (vs. NHE) (the details of estimation is provided in the electronic supplementary information), and the VB and CB of g-C_3N_4 are located at 1.53 and -1.17 eV (vs. NHE).[18] Rh-B shows the highest absorption

at wavelength of 553 nm in the visible region with E_0= -1.42 V (vs. NHE).[33] Therefore, Rh-B and g-C_3N_4 can be excited by visible light (λ ≥ 400 nm). Due to the large offset of energy level (at least 1.65 eV) at the Rh-B/$Bi_2O_2CO_3$ interfaces, photogenerated electrons move rapidly from Rh-B to BOC in a

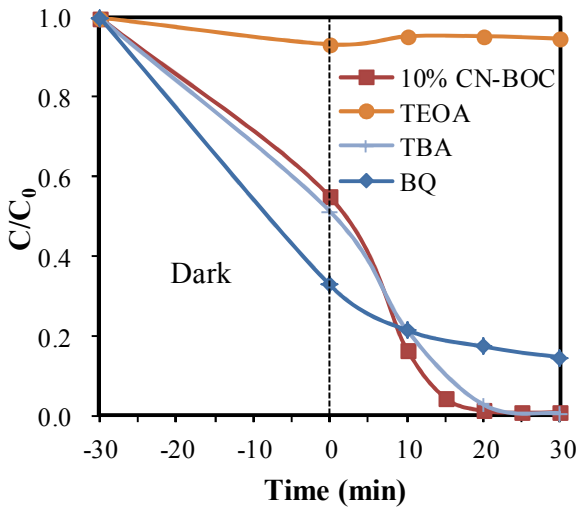

Figure 8. Photocatalytic degradation of Rh-B over 10% CN-BOC (with heterojunctions) as well as with the addition of BQ, TBA and TEOA.

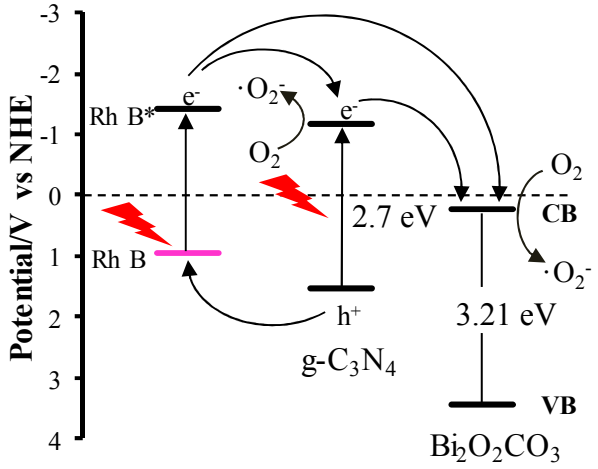

Scheme 1. Mechanism of charge separation and photocatalytic process over CN-BOC photocatalysts under visible light irradiation

thermodynamically favorable manner. Furthermore, some electrons generated in g-C_3N_4 excitation move into the BOC structure quickly since the CB of BOC is more negative than that of g-C_3N_4, making charge separation efficient and reducing the probability of electron-hole recombination. The transferred electrons can be taken up by surface dioxygen to give $\bullet O_2^-$, while the holes generated in g-C_3N_4 can directly oxidize the adsorbed dyes. Hence, the significant enhancement of photosensitized activity is attributed to the high charge-separation efficiency due to the hybrid effect of Rh-B, $Bi_2O_2CO_3$ and g-C_3N_4.

Photocatalytic stability

The stability of the 10% CN-BOC composite was evaluated in a recycle test of five runs (Figure 9). There is only slight decrease of degradation rate after the fourth run, and complete degradation of Rh-B can still be achieved within 30 min. The lowering of photocatalytic efficiency is ascribable to the accumulation of residual Rh-B in the inner pores. The reused catalysts was dried and characterized by the XRD and FT-IR techniques. Apparently, there was no change of phase structure after the 5 runs (Figure 1c and e). As shown in the FT-IR spectra (Figure S6, ESI), the reused sample shows spectrum similar to that of the fresh sample. Since there is no detection of the characteristic peaks belonging to Rh-B, it is deduced that there is complete degradation of dye molecules. The results demonstrate that the as-prepared g-C_3N_4-$Bi_2O_3CO_3$ composite is highly stable in the photosensitized degradation process.

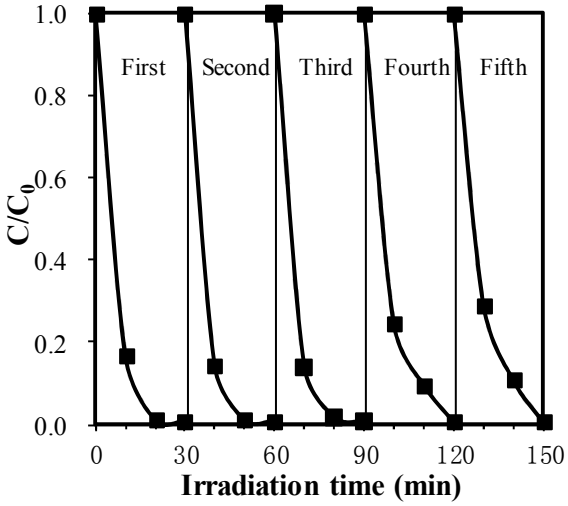

Figure 9. Cycles of Rh-B degradation over 10% CN-BOC under visible light irradiation (λ≥ 400 nm)

Conclusions

Flower-like $Bi_2O_2CO_3$ and g-C_3N_4-$Bi_2O_2CO_3$ microspheres with high adsorption ability were fabricated via a facile method. The visible-light-driven photocatalytic process of $Bi_2O_2CO_3$ was proved to be a dye-sensitized one. To enhance its activity under visible light, we modified $Bi_2O_2CO_3$ with g-C_3N_4, and the amount of g-C_3N_4 for optimal activity is 10 wt.%. The g-C_3N_4-$Bi_2O_2CO_3$ composite shows good photocatalytic activity and stability towards the degradation of cationic (Rh-B, MB, CV) as well as anionic (MO) dyes. The high visible-light activity is ascribed to g-C_3N_4 being excellent in terms of dye sensitivity. It is deduced that the matching of the energy levels of dye, $Bi_2O_2CO_3$ and g-C_3N_4 facilitates the transfer of photogenerated electrons and holes, leading to the superior photocatalytic activity as a result.

Acknowledgements

The authors thank the National Natural Science Foundation of China (Grant Nos. U1162109, J0830415, and J1210040), the Program for New Century Excellent Talents in Universities (NCET-10-0371), the Program for Changjiang Scholars and Innovative Research Team in Universities (IRT1238), as well as the Fundamental Research Funds for the Central Universities for financial supports. C.T. Au thanks the Hunan University for an adjunct professorship.

Notes and references

[a] State Key Laboratory of Chemo/Biosensing and Chemometrics, College of Chemistry and Chemical Engineering, Hunan University, Changsha 410082, Hunan, People's Republic of China
[b] Department of Chemistry, Hong Kong Baptist University, Room T1214, Cha Chi-Ming Science Tower, Kowloon Tong, Hong Kong
[c] The authors contributed equally
* Corresponding author: Phone (Fax): 86-731-88821171. E-mail address: sf_yin@hnu.edu.cn

Electronic Supplementary Information (ESI) available: [Absorption spectra of Rh-B with irradiation time over BOC and 10% CN-BOC under visible light irradiation; Temporal absorption spectra of methylene blue solution and violet solution over 10% CN-BOC under visible light irradiation; Degradation rates of methyl orange under visible light irradiation in the presence of g-C_3N_4, $Bi_2O_2CO_3$ and 10% CN-BOC; FT-IR spectrum of (a) 10% CN-BOC, (b) 10% CN-BOC after five recycle experiments, (c) Rh-B]. See DOI: 10.1039/b000000x/

1 M. R. Hoffmann, S. T. Martin, W. Choi and D. W. Bahnemann, *Chem. Rev.*, 1995, **95**, 69-96.
2 A. Kubacka, M. Fernández-García, and G. Colón, *Chem. Rev.*, 2012, **112**, 1555-1614.
3 S. Y. Chai, Y. J. Kim, M. H. Jung, A. K. Chakraborty, D. Jung and W. I. Lee, *J. Catal.*, 2009, **262**, 144-149.
4 S. Shenawi-Khalil, V. Uvarov, S. Fronton, I. Popov and Y. Sasson, *J. Phys. Chem. C*, 2012, **116**, 11004-11012.
5 L. Chen, R. Huang, Y. J. Ma, S. L. Luo, C. T. Au and S. F. Yin, *RSC Adv.*, 2013, **3**, 24354-24361.
6 L. Chen, S. F. Yin, S. L. Luo, R. Huang, Q. Zhang, T. Hong and C. T. Au, *Ind. Eng. Chem. Res.*, 2012, **51**, 6760-6768.
7 L. Chen, Q. Zhang, R. Huang, S. F. Yin, S. L. Luo and C. T. Au, *Dalton Trans.*, 2012, **41**, 9513-9518.
8 W. Li, D. Li, S. Meng, W. Chen, X. Fu and Y. Shao, *Environ. Sci. Technol.* 2011, **45**, 2987-2993.
9 D. H. Wang, G. Q. Gao, Y. W. Zhang, L. S. Zhou, A. W. Xu and W. Chen, *Nanoscale*, 2012, **4**, 7780-7785.
10 J. Tang, H. Zhao, G. Li, Z. Lu, S. Xiao and R. Chen, *Ind. Eng. Chem. Res.*, 2013, **52**, 12604-12612.
11 Y. S. Xu and W. D. Zhang, *Appl. Catal. B: Environ.*, 2013, **140-141**, 306-316.
12 J. Hu, W. Cheng, S. Huang, D. Wu and Z. Xie, *Appl. Phys. Lett.*, 2006, **89**, 261117, 1-3.
13 Y. Wang, R. Shi, J. Lin and Y. Zhu, *Energy Environ. Sci.*, 2011, **4**, 2922-2929.
14 C. Pan, J. Xu, Y. Wang, D. Li and Y. Zhu, *Adv. Funct. Mater.*, 2012, **22**, 1518-1524.
15 L. Ye, J. Liu, Z. Jiang, T. Peng and L. Zan, *Appl. Catal. B: Environ.*, 2013, **142-143**, 1-7.
16 Y. Tian, B. Chang, J. Lu, J. Fu, F. Xi and X. Dong, *ACS Appl. Mater. Interfaces*, 2013, **5**, 7079-7085.
17 G. Liao, S. Chen, X. Quan, H. Yu and H. Zhao, *J. Mater. Chem.*, 2012, **22**, 2721-2726.
18 S. C. Yan, Z. S. Li and Z. G. Zou, *Langmuir*, 2010, **26**, 3894-3901.
19 S. C. Yan, Z. S. Li and Zou, Z. G. *Langmuir*, 2009, **25**, 10397-10401.
20 G. Zhang, J. Zhang, M. Zhang and X. Wang, *J. Mater. Chem.*, 2012, **22**, 8083-8091.
21 J. Liu, T. Zhang, Z. Wang, G. Dawson and W. Chen, *J. Mater. Chem.*, 2011, **21**, 14398-14401.
22 L. Liu, D. Ma, H. Zheng, X. Li, M. Cheng and X. Bao, *Microporous Mesoporous Mater.*, 2008, **110**, 216-222.
23 G. T. Zou, *Appl. Phys. A: Mater. Sci. Process.*, 2009, **94**, 387-392.
24 G. E. Tobon-Zapata, S. B. Etcheverry and E. J. Baran, *J. Mater. Sci. Lett.*, 1997, **16**, 656-657.
25 Q. Xiang, J. Yu and M. Jaroniec, *J. Phys. Chem. C*, 2011, **115**, 7355-7363.
26 H. Cheng, B. Huang, K. Yang, Z. Wang, X. Qin, X. Zhang and Y. Dai, *ChemPhysChem*, 2010, **11**, 2167-2173.
27 Y. Liu, Z. Wang, B. Huang, K. Yang, X. Zhang, X. Qin and Y. Dai, *Appl. Surf. Sci.*, 2010, **257**, 172-175.
28 X. Wang, K. Maeda, A. Thomas, K. Takanabe, G. Xin, J. M. Carlsson, K. Domen and M. Antonietti, *Nat. Mater.*, 2009, **8**, 76-80.
29 F. Dong, L. Wu, Y. Sun, M. Fu, Z. Wu and S. C. Lee, *J. Mater. Chem.*, 2011, **21**, 15171-15174.
30 G. V. Buxton, C. L. Greenstock, W. P. Helman and A. B. Ross, *J. Phys. Chem. Ref. Data*, 1988, **17**, 513-535
31 Y. Zhang, N. Zhang, Z. Tang and Y. Xu, *Chem. Sci*., 2013, **4**, 1820-1824.
32 A. H. Nethercot, *Phys. Rev. Lett.*, 1974, **33**, 1088-1091
33 Z. G. Xiong, L. L. Zhang, J. Z. Ma and X. S. Zhao, *Chem. Commun.*, 2010, **46**, 6099-6101

